

Gravitational wave emission from rotating superfluid neutron stars

D. I. Jones^{1*}

¹*School of Mathematics, University of Southampton, Southampton SO17 1BJ*

11 December 2009

ABSTRACT

In this paper we investigate the effect of a pinned superfluid component on the gravitational wave emission of a steadily rotating deformed neutron star. We show that the superfluid pinning allows the possibility for there to be gravitational wave emission at both the stellar spin frequency Ω and its first harmonic, 2Ω . This contrasts with the conventional case where there is no pinned superfluidity, where either only the 2Ω harmonic is present, or else the star undergoes precession, a feature which is not believed to be common in the known pulsar population. This work motivates the carrying out of gravitational wave searches where both the Ω and 2Ω harmonics are searched for, even in targeted searches for waves from known pulsars which aren't observed to precess. Observation of such a two-component signal would provide evidence in favour of pinned superfluidity inside the star.

Key words: gravitational waves – stellar dynamics – stars: neutron – pulsars: general – stars: rotation

1 INTRODUCTION

Spinning neutron stars are a source of potentially detectable gravitational waves, and so are of interest for the current generation of laser interferometer gravitational wave detectors (Abbott et al. 2009a; Acernese et al. 2008; Grote 2008). A number of searches have already been performed, so far producing upper limits on the gravitational wave emission (Abbott et al. 2004, 2005a,b, 2007a,b, 2008a,b, 2009b,c). A highlight was the result of Abbott et al. (2008b), where the energy being emitted in the gravitational wave channel by the Crab pulsar was shown to be no more than 6% of the total spin-down energy budget.

Most gravitational wave searches have assumed emission at a single gravitational wave frequency. In the case of searches targeting pulsars of known spin frequency Ω , the gravitational wave signal has been assumed to be at frequency 2Ω (see e.g. Abbott et al. (2007a)). This is exactly the sort of emission to be expected from a steadily spinning triaxial body, rotating about one of the principal axes of its moment of inertia tensor (Shapiro & Teukolsky 1983). The necessary deformation could be supported by strains in the solid crust, or by strong internal magnetic fields (Ushomirsky, Cutler & Bildsten 2000; Haskell et al. 2008). More complicated gravitational wave emission occurs, with multiple harmonics, if the spin and principal axes are misaligned (Zimmermann & Szedenits, Jr. 1979; Zimmermann 1980; Jones & Andersson 2002; Van Den Broeck 2005). However, such free precession would produce modulations in the time of arrival, polarisation, and beam shape of the radio pulsations (see Jones & Andersson (2001) and references therein). It is the absence of clear evidence of precession in gravitational wave candidates that has led to most searches assuming a single monochromatic signal. A notable exception was the analysis for the Crab pulsar presented by Abbott et al. (2008b), where a small frequency band around 2Ω was searched, motivated in part by the possibility of precession, and in part by the possibility of gravitational wave emission occurring from a stellar component with spin frequency slightly different from the radio-pulsation-producing outer crust.

In this paper we revisit the issue of gravitational wave emission from rotating stars, by allowing for a superfluid component within the star. There are strong reasons to believe that superfluids exist in neutron stars, and that they have an effect on the stellar dynamics (Sauls 1989). Superfluids rotate by forming an array of vortices, with the number of vortices per unit

* Email: D.I.Jones@soton.ac.uk

area being proportional to the rotation rate. An interaction between these vortices and the charged component of the star is believed to result in ‘pinning’ of these vortices, preventing that portion of the superfluid that is pinned from participating in the smooth spin-down of the star. Instead, the spin rate of the pinned superfluid remains constant, so that a spin lag builds up between the superfluid and the pinned vortices. When this lag becomes sufficiently large, some mechanism is believed to result in a catastrophic unpinning, spinning up the star’s charged component, and producing one of the well known pulsar glitches.

As was pointed out by Shaham (1977), in addition to producing glitches, a pinned superfluid component also has important repercussions for the precessional dynamics of a star. Classically, the free precession of a rigid body is determined by the principal moments of inertia (I_1, I_2, I_3). However, Shaham showed that a pinned superfluid alters the motion, effectively acting as a large gyroscope, ‘sewn’ into the body of the star. If the star is set into precession, the angular momentum vector of the pinned superfluid follows the wobbling motion of the star, and this must be included in the solution of the Euler rigid body equations of motion.

The detailed form of the free precession that then occurs is given in Shaham (1977). We will not concern ourselves with the corresponding gravitational wave emission here. Instead, we will confine our attention to the allowed non-precessional motion of such a star, and the consequent gravitational wave emission. The key point is this: if one allows for the possibility of the superfluid pinning along an axis that isn’t one of the principal axes of the star’s moment of inertia tensor, even the non-precessing motion is interesting: despite rotating steadily at rate Ω , there is gravitational wave emission at both Ω and 2Ω . The relative strengths are dependent on the moments of inertia and relative orientations of the stellar components. Basically, this motion is possible because the moment of inertia of the pinned superfluid is likely to be many orders of magnitude greater than the asymmetries ($I_2 - I_1, I_3 - I_2, I_3 - I_1$), which (as we show below) means that, to a good approximation, the non-precessing motion corresponds to rotation about the superfluid pinning axis, not to rotation about any one of the principal axes. This means that even in the absence of any observed precession in the radio data, a given star might possibly be radiating at both Ω and 2Ω , motivating the carrying out of gravitational wave searches that account for this.

There are two different locations where superfluid pinning may occur in a neutron star (see e.g. Sauls (1989)). One location is the inner crust, the other is the core, and the physical conditions in the two regimes are very different. In the crust, pinning may occur because of an interaction between the vortices and the nuclear lattice (Anderson & Itoh 1975). In the case of small relative velocities between superfluid and vortex, the pinning may be strong enough to prevent motion of the vortices with respect to the lattice; an explicit model of this was presented recently by Link (2009). This crustal superfluid is believed to make up only a few percent of the star’s total moment of inertia. The other possible pinning location is the core, where there is believed to be a strong interaction between the vortices and magnetic flux tubes (Ruderman 1976, 1991a,b). In this case, the bulk of the star’s moment of inertia might be a pinned superfluid. For the most part, the exact location and cause of the pinning is not important for our purposes—what matters is that the pinning exists and is maintained for periods longer than the gravitational wave observation time. The long separation between glitches in young pulsars indicates that this may indeed be the case (Lyne & Graham-Smith 1998).

The plan of this paper is as follows. In section 2 we present our basic rigid body stellar model and derive the form of the non-precessional solution. In section 3 we calculate the corresponding gravitational wave emission, count the number of parameters required to describe the signal, and discuss the angular pattern of the emission. In section 4 we show that the results obtained still apply when the assumption of rigidity is relaxed to one of elasticity. In section 5 we discuss what might limit the wave emission and what mechanisms might prevent our model being realised. In section 6 we talk about two other (non-superfluid) mechanisms that can lead to radiation at multiple frequencies, and show they are likely to be less important than the superfluid pinning mechanism. Finally, in section 7, we speculate as to how the sorts of deformed stars considered in this paper might arise in nature.

2 BASIC MODEL

We will begin by following Shaham (1977), extending his treatment slightly by modelling a star consisting of a triaxial rigid ‘crust’ and a pinned superfluid component of spherical moment of inertia (Shaham assumed a biaxial crust). Note that here, and for the entirety of this paper, by ‘crust’ we mean not just the outer solid phase but all parts of the star apart from the pinned superfluid. Referring our equations to the crust’s body frame and denoting by $\{n_a^1, n_a^2, n_a^3\}$ unit vectors along the crust’s principal axes, the crust’s moment of inertia tensor is

$$I_{ab}^C = I_1^C n_a^1 n_b^1 + I_2^C n_a^2 n_b^2 + I_3^C n_a^3 n_b^3, \quad (1)$$

while the superfluid’s is

$$I_{ab}^{SF} = I^{SF} \delta_{ab}. \quad (2)$$

The star’s total angular momentum is then the sum of the angular momenta of the two components:

$$J_a = I_{ab}^C \Omega_b^C + I_a^{\text{SF}} \Omega_a^{\text{SF}}, \quad (3)$$

where Ω_a^C and Ω_a^{SF} are the crustal and superfluid angular velocities, respectively. Writing out the components of J_a explicitly:

$$J_1 = I_1^C \Omega_1^C + I_1^{\text{SF}} \Omega_1^{\text{SF}}, \quad (4)$$

$$J_2 = I_2^C \Omega_2^C + I_2^{\text{SF}} \Omega_2^{\text{SF}}, \quad (5)$$

$$J_3 = I_3^C \Omega_3^C + I_3^{\text{SF}} \Omega_3^{\text{SF}}. \quad (6)$$

If the pinned superfluid has a rotation axis given by the spherical polar angles $(\theta^{\text{SF}}, \phi^{\text{SF}})$ with respect to the crust frame then

$$\Omega_a^{\text{SF}} = \Omega^{\text{SF}} (\sin \theta^{\text{SF}} \cos \phi^{\text{SF}} n_a^1 + \sin \theta^{\text{SF}} \sin \phi^{\text{SF}} n_a^2 + \cos \theta^{\text{SF}} n_a^3). \quad (7)$$

The Euler equation of motion is

$$\frac{dJ_a}{dt} + \epsilon_{abc} \Omega_b^C J_c = 0, \quad (8)$$

where the time derivative is evaluated in the crust frame. Writing out the components explicitly we obtain:

$$I_1^C \dot{\Omega}_1^C + \Omega_2^C \Omega_3^C (I_3^C - I_2^C) + (\Omega_2^C \cos \theta^{\text{SF}} - \Omega_3^C \sin \theta^{\text{SF}} \sin \phi^{\text{SF}}) I^{\text{SF}} \Omega^{\text{SF}} = 0, \quad (9)$$

$$I_2^C \dot{\Omega}_2^C + \Omega_3^C \Omega_1^C (I_1^C - I_3^C) + (\Omega_3^C \sin \theta^{\text{SF}} \cos \phi^{\text{SF}} - \Omega_1^C \cos \theta^{\text{SF}}) I^{\text{SF}} \Omega^{\text{SF}} = 0, \quad (10)$$

$$I_3^C \dot{\Omega}_3^C + \Omega_1^C \Omega_2^C (I_2^C - I_1^C) + (\Omega_1^C \sin \theta^{\text{SF}} \sin \phi^{\text{SF}} - \Omega_2^C \sin \theta^{\text{SF}} \cos \phi^{\text{SF}}) I^{\text{SF}} \Omega^{\text{SF}} = 0. \quad (11)$$

The non-precessing solution is obtained by setting $dJ_a/dt = 0$ in equation (8), which in turn implies $\epsilon_{abc} \Omega_b^C J_c = 0$, i.e. Ω_a^C is parallel to J_a , so that the crust rotates steadily about the fixed angular momentum vector. Equations (9)–(11) then reduce to

$$\Omega_2^C \Omega_3^C (I_3^C - I_2^C) + (\Omega_2^C \cos \theta^{\text{SF}} - \Omega_3^C \sin \theta^{\text{SF}} \sin \phi^{\text{SF}}) I^{\text{SF}} \Omega^{\text{SF}} = 0, \quad (12)$$

$$\Omega_3^C \Omega_1^C (I_1^C - I_3^C) + (\Omega_3^C \sin \theta^{\text{SF}} \cos \phi^{\text{SF}} - \Omega_1^C \cos \theta^{\text{SF}}) I^{\text{SF}} \Omega^{\text{SF}} = 0, \quad (13)$$

$$\Omega_1^C \Omega_2^C (I_2^C - I_1^C) + (\Omega_1^C \sin \theta^{\text{SF}} \sin \phi^{\text{SF}} - \Omega_2^C \sin \theta^{\text{SF}} \cos \phi^{\text{SF}}) I^{\text{SF}} \Omega^{\text{SF}} = 0. \quad (14)$$

If we regard $\Omega^{\text{SF}}, \theta^{\text{SF}}, \phi^{\text{SF}}$ as fixed, as is appropriate for a perfectly pinned superfluid, these equations then have a one-parameter family of solutions, which we will parameterise in terms of Ω_3^C . Then we find

$$\Omega_1^C = \Omega_3^C \frac{I^{\text{SF}} \Omega^{\text{SF}} \sin \theta^{\text{SF}} \cos \phi^{\text{SF}}}{I_{31} \Omega_3^C + I^{\text{SF}} \Omega^{\text{SF}} \cos \theta^{\text{SF}}}, \quad (15)$$

$$\Omega_2^C = \Omega_3^C \frac{I^{\text{SF}} \Omega^{\text{SF}} \sin \theta^{\text{SF}} \sin \phi^{\text{SF}}}{I_{32} \Omega_3^C + I^{\text{SF}} \Omega^{\text{SF}} \cos \theta^{\text{SF}}}, \quad (16)$$

having defined

$$I_{31} \equiv I_3^C - I_1^C, \quad (17)$$

$$I_{32} \equiv I_3^C - I_2^C, \quad (18)$$

$$I_{21} \equiv I_2^C - I_1^C. \quad (19)$$

To fix the orientation of the body with respect to the inertial frame, define a set of three Euler angles (θ, ϕ, ψ) which connect the body frame to the inertial frame in the standard manner, as described in Landau & Lifshitz (1976) and illustrated in Figure 1. Then

$$\Omega_1^C = \dot{\phi} \sin \theta \sin \psi + \dot{\theta} \cos \psi, \quad (20)$$

$$\Omega_2^C = \dot{\phi} \cos \theta \cos \psi - \dot{\theta} \sin \psi, \quad (21)$$

$$\Omega_3^C = \dot{\phi} \cos \theta + \dot{\psi}. \quad (22)$$

Our non-precessing solution has all components of Ω_a^C constant, and so equations (20) and (21) imply that θ and ψ must be constant, leaving

$$\Omega_1^C = \dot{\phi} \sin \theta \sin \psi, \quad (23)$$

$$\Omega_2^C = \dot{\phi} \cos \theta \cos \psi, \quad (24)$$

$$\Omega_3^C = \dot{\phi} \cos \theta. \quad (25)$$

These can be inverted easily to give

$$\tan \theta = \frac{[(\Omega_1^C)^2 + (\Omega_2^C)^2]^{1/2}}{\Omega_3^C}, \quad (26)$$

$$\phi = \Omega^C t + \phi_0, \quad (27)$$

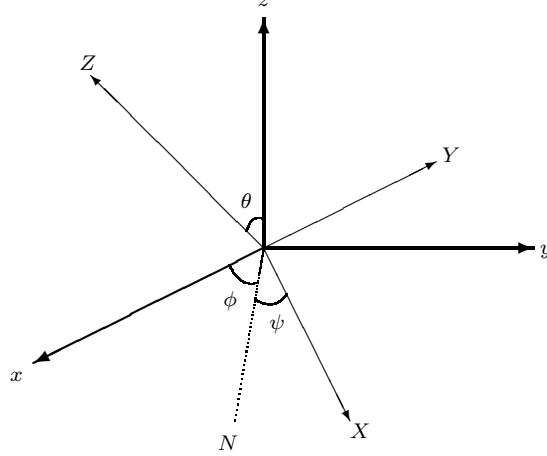


Figure 1. The orientation of our body is specified by the three standard Euler angles (θ, ϕ, ψ) , as labelled above. The fixed inertial-frame axes are denoted by (x, y, z) , while the rotating body-frame axes are denoted by (X, Y, Z) . The so-called line of nodes, N , lies along the intersection of the xy and XY planes.

$$\tan \psi = \frac{\Omega_1^C}{\Omega_2^C}. \quad (28)$$

The angles θ and ψ are constant, while ϕ is a linearly increasing function of time—it is this angle that generates the rotation. Elimination of Ω_1^C and Ω_2^C in favour of Ω_3^C using equations (15) and (16) gives

$$\tan \theta = \tan \theta^{\text{SF}} \left[\cos^2 \phi^{\text{SF}} \left(1 + \frac{I_{31}\Omega_3^C}{I^{\text{SF}}\Omega_3^{\text{SF}}} \right)^{-2} + \sin^2 \phi^{\text{SF}} \left(1 + \frac{I_{32}\Omega_3^C}{I^{\text{SF}}\Omega_3^{\text{SF}}} \right)^{-2} \right]^{1/2}, \quad (29)$$

$$\phi = \Omega_3^C t \left\{ \tan^2 \theta^{\text{SF}} \left[\cos^2 \phi^{\text{SF}} \left(1 + \frac{I_{31}\Omega_3^C}{I^{\text{SF}}\Omega_3^{\text{SF}}} \right)^{-2} + \sin^2 \phi^{\text{SF}} \left(1 + \frac{I_{32}\Omega_3^C}{I^{\text{SF}}\Omega_3^{\text{SF}}} \right)^{-2} \right] + 1 \right\}^{1/2} + \phi_0, \quad (30)$$

$$\tan \psi = \tan(\pi/2 - \phi^{\text{SF}}) \left[1 + \frac{I_{32}\Omega_3^C}{I^{\text{SF}}\Omega_3^{\text{SF}}} \right] \left[1 + \frac{I_{31}\Omega_3^C}{I^{\text{SF}}\Omega_3^{\text{SF}}} \right]^{-1}, \quad (31)$$

where ϕ_0 is a constant. Clearly, there is a rather complicated relationship between the orientation of the body with respect to the inertial frame and the parameters $\Omega_3^C, \Omega_3^{\text{SF}}, \theta^{\text{SF}}, \phi^{\text{SF}}$.

However, we can simplify the above. The asymmetries I_{31}, I_{32} are sourced by crustal strains or magnetic fields, and so are likely to be very small. In the case of crustal strains, Haskell et al. (2006), following the work of Ushomirsky, Cutler & Bildsten (2000), estimated *maximum* deformations of approximately

$$\frac{\Delta I}{10^{45} \text{ g cm}^2} \approx 3 \times 10^{-5} \left(\frac{u_{\text{break}}}{0.1} \right), \quad (32)$$

where u_{break} denotes the breaking strain of the crust. Recent molecular dynamics calculations (Horowitz & Kadau 2009) estimate this breaking to strain to be approximately 0.1. Note that the above crustal deformation is an upper bound as it assumes the crust is maximally strained. In the case of an internal magnetic field of strength $\sim B$ a naive estimate is (Jones 2002)

$$\frac{\Delta I}{10^{45} \text{ g cm}^2} \approx 10^{-12} \left(\frac{B}{10^{12} \text{ G}} \right)^2, \quad (33)$$

although more detailed calculations show the result depends on the assumed field geometry (Bonazzola & Gourgoulhon 1996; Haskell et al. 2008; Ciolfi et al. 2009; Lander & Jones 2009) and on the superconducting nature of the core (see Cutler (2002) and references therein).

On the other hand, the moment of inertia of the superfluid is relatively large: $I_{\text{SF}}/I \sim 10^{-2}$ for crustal pinning, $I^{\text{SF}}/I \sim 1$ for core pinning (Sauls 1989). We can therefore make use of the inequalities

$$\frac{I_{31}\Omega_3^C}{I_{\text{SF}}\Omega_3^{\text{SF}}} \ll 1 \quad \frac{I_{32}\Omega_3^C}{I_{\text{SF}}\Omega_3^{\text{SF}}} \ll 1 \quad (34)$$

to simplify our expressions for the Euler angles

$$\theta \approx \theta^{\text{SF}}, \quad (35)$$

$$\phi \approx \frac{\Omega_3^C t}{\cos \theta^{\text{SF}}} + \phi_0, \quad (36)$$

$$\psi \approx \pi/2 - \phi^{\text{SF}}, \quad (37)$$

This shows that the star rotates about an axis very close to n_a^{SF} . So, after having gone through a careful analysis, the basic picture is very simple: the star rotates steadily about an axis very close to the superfluid pinning axis. From this point on we will simplify our notation slightly, writing $(\Omega_a^C \Omega_a^C)^{1/2}$ simply as Ω , the observed stellar spin frequency.

3 GRAVITATIONAL WAVE EMISSION

3.1 Calculation of the gravitational wave signal

Having obtained the Euler angles (θ, ϕ, ψ) giving the orientation of the body with respect to the inertial frame it is straightforward to calculate the corresponding gravitational wave emission. To do so we will calculate the source's multipole moments, as described by Thorne (1980); this will make clear the separation between the frequency harmonics and will also be useful in discussing maximum possible wave amplitudes in section 3.3. The multipole moments of the source are complex scalars defined by integrals over the star's density field ρ :

$$Q_{lm} = \int \rho r^l Y_{lm}^* d^3x. \quad (38)$$

When the density field is written as the sum $\rho = \Sigma \delta \rho_{lm} Y_{lm}$ this reduces to

$$Q_{lm} = \int \delta \rho_{lm}(r) r^{l+2} dr. \quad (39)$$

When the body has orientation θ, ϕ, ψ relative to the inertial axes we find

$$Q_{21} = \frac{1}{2} \sqrt{\frac{15}{2\pi}} e^{-i\phi} [-I_{21} \sin 2\psi \sin \theta - i \sin 2\theta (I_{21} \cos^2 \psi - I_{31})], \quad (40)$$

$$Q_{22} = \frac{1}{2} \sqrt{\frac{15}{2\pi}} e^{-2i\phi} [I_{21} (\cos^2 \psi \cos^2 \theta - \sin^2 \psi) + I_{31} \sin^2 \theta - i I_{21} \sin 2\psi \cos \theta]. \quad (41)$$

The Q_{21} multipole moment generates radiation at the spin frequency Ω , while the Q_{22} multipole moment generates radiation at 2Ω .

In calculating the gravitational wave emission, we will consider an observer a distance r from the star whose coordinate system (X, Y, Z) is obtained from the inertial (x, y, z) frame by a rotation through an inclination angle ι about the inertial x -axis, followed by a translation through a distance r along OZ . The gravitational wave then propagates along OZ and, within the mass quadrupole approximation to general relativity, the two polarisations which make up the transverse traceless wave field are

$$h_+^{\Omega} = -\frac{\Omega^2}{r} \sin \iota \cos \iota \{ [I_{21} \cos^2 \psi - I_{31}] \sin 2\theta \cos \phi - I_{21} \sin 2\psi \sin \theta \sin \phi \}, \quad (42)$$

$$h_{\times}^{\Omega} = -\frac{\Omega^2}{r} \sin \iota \{ I_{21} \sin 2\psi \sin \theta \cos \phi + (I_{21} \cos^2 \psi - I_{31}) \sin 2\theta \sin \phi \}, \quad (43)$$

$$h_+^{2\Omega} = -\frac{2\Omega^2}{r} (1 + \cos^2 \iota) \{ [I_{21} (\cos^2 \psi \cos^2 \theta - \sin^2 \psi) + I_{31} \sin^2 \theta] \cos 2\phi - I_{21} \sin 2\psi \cos \theta \sin 2\phi \}, \quad (44)$$

$$h_{\times}^{2\Omega} = -\frac{2\Omega^2}{r} 2 \cos \iota \{ I_{21} \sin 2\psi \cos \theta \cos 2\phi + [(I_{21} (\cos^2 \psi \cos^2 \theta - \sin^2 \psi) + I_{31} \sin^2 \theta) \sin 2\phi] \}. \quad (45)$$

These equations, together with the equations (29)–(31) (or alternatively the approximate equations (35)–(37)) then give a complete specification of the gravitational field. As anticipated, there are harmonics at both Ω and 2Ω .

3.2 Counting the number of parameters

The actual signal received by a detector can be written as

$$h(t) = F_+(t)h_+(t) + F_{\times}(t)h_{\times}(t), \quad (46)$$

where F_+ and F_\times are the beam pattern factors whose form can be found in Jaranowski, Królak & Schutz (1998). They depend upon the detector location, source position on the sky, and on the orientation of the source's spin axis. This introduces three unknown parameters over and above those appearing in the expressions for h_+ and h_\times , specifically the source's location on the sky (which can be specified by right ascension α and declination δ), and an angle giving the projection of the source's spin axis on the plane perpendicular to the line-of-sight (which can be specified by the polarisation angle ψ_{pol}).

We can now count the number of parameters required to reconstruct the full signal. Let us first examine two special cases, to demonstrate consistency with previously published results.

If we put $\theta = 0$ in (42)–(45) we obtain

$$h_+ = -\frac{2\Omega^2}{r} I_{21} (1 + \cos^2 i) \cos 2(\phi + \psi), \quad (47)$$

$$h_\times = -\frac{2\Omega^2}{r} I_{21} 2 \cos i \sin 2(\phi + \psi). \quad (48)$$

This corresponds to a triaxial star spinning about a principal axis; it is the sort of signal that has been assumed in many gravitational wave searches (see e.g. Abbott et al. (2007a)). A possible choice of parameters to describe the signal is:

$$\left\{ \frac{\Omega^2 I_{21}}{r}, \Omega, (\phi + \psi)_0, \iota, \psi_{\text{pol}}, \alpha, \delta \right\}. \quad (49)$$

In this case there are 7 parameters (note that in this case the angles ϕ and ψ are degenerate, and only their sum appears in the waveform). There is radiation only at the 2Ω harmonic.

If we put $I_{21} = 0$ in (42)–(45) we obtain

$$h_+^\Omega = \frac{\Omega^2}{r} \sin \iota \cos \iota I_{31} \sin 2\theta \cos \phi, \quad (50)$$

$$h_\times^\Omega = \frac{\Omega^2}{r} \sin \iota I_{31} \sin 2\theta \sin \phi, \quad (51)$$

$$h_+^{2\Omega} = -\frac{2\Omega^2}{r} (1 + \cos^2 \iota) I_{31} \sin^2 \theta \cos 2\phi, \quad (52)$$

$$h_\times^{2\Omega} = -\frac{2\Omega^2}{r} 2 \cos \iota I_{31} \sin^2 \theta \sin 2\phi. \quad (53)$$

This is identical to the wave field of a precessing biaxial star, and therefore is of exactly the same form as given in Zimmermann & Szedenits, Jr. (1979) and Jaranowski, Królak & Schutz (1998). Note, however, that in our case the motion is not one of free precession—the star rotates steadily about the fixed angular momentum vector, with no superimposed rotation about the crust's symmetry axis. A possible choice of parameters is:

$$\left\{ \frac{\Omega^2 I_{31}}{r}, \Omega, \phi_0, \theta, \iota, \psi_{\text{pol}}, \alpha, \delta \right\}. \quad (54)$$

In this case there are 8 parameters, with the angle θ being the extra parameter as compared to the case considered above. There is radiation at both the Ω and 2Ω harmonics, and θ controls the relative strength of these. In the limit of small θ , they scale as θ and θ^2 respectively, so the Ω harmonic can dominate, but both go to zero (at fixed I_{31}) in the limit $\theta \rightarrow 0$.

Finally, consider the general case. The wave field is then as given in equations (42)–(45). A possible choice of parameters is

$$\left\{ \frac{\Omega^2 I_{21}}{r}, \frac{I_{31}}{I_{21}}, \Omega, \phi_0, \theta, \psi, \iota, \psi_{\text{pol}}, \alpha, \delta \right\}. \quad (55)$$

In this case there are 10 parameters, with the ratio I_{31}/I_{21} and the angle ψ being the extra parameters as compared to the case above. In general, there is radiation at both Ω and 2Ω , but the relative strengths depends on the parameters in a rather complicated way. Let us consider the extremes. There are solutions where the star radiates only at 2Ω , with the signal being proportional to one of I_{21}, I_{31}, I_{32} . These correspond to the familiar case of rotation of a triaxial star about a principal axis. More interestingly, there also exist solutions where the star radiates only at Ω . The solutions are:

$$\sin \psi = 0, \quad \tan \theta = \sqrt{-\frac{I_{21}}{I_{31}}}, \quad |Q_{21}| = \sqrt{\frac{15}{2\pi}} \sqrt{-I_{21} I_{31}}, \quad (56)$$

$$\cos \psi = 0, \quad \sin \theta = \sqrt{+\frac{I_{21}}{I_{31}}}, \quad |Q_{21}| = \sqrt{\frac{15}{2\pi}} \sqrt{I_{21} I_{32}}, \quad (57)$$

$$\cos \theta = 0, \quad \sin \psi = \sqrt{+\frac{I_{31}}{I_{21}}}, \quad |Q_{21}| = \sqrt{\frac{15}{2\pi}} \sqrt{I_{31} I_{32}}. \quad (58)$$

Clearly, to obtain radiation only at the Ω harmonic, special values of the parameters are necessary. For general values of the parameters, there will be radiation at both harmonics.

3.3 Gravitational wave amplitudes

Let us now examine the relative strengths at which the two quadrupole moments can radiate. As noted by Ushomirsky, Cutler & Bildsten (2000), the Q_{22} perturbations are somewhat more efficient gravitational wave emitters, in the sense that for a given magnitude of the quadrupole moment (i.e. $|Q_{21}| = |Q_{22}|$), the energy flux in the 2Ω radiation is greater than that in the Ω radiation. To see this we can calculate the inclination-angle (ι) dependent gravitational wave energy flux using (Thorne 1980)

$$F = \frac{1}{32\pi} \langle \dot{h}_{ab}^{\text{TT}} \dot{h}_{ab}^{\text{TT}} \rangle, \quad (59)$$

where the angle brackets denote a time average over several periods. This gives the following when written in terms of multipole moments:

$$F_{\Omega}(\iota) = \frac{1}{60} \frac{\Omega^6}{r^2} |Q_{21}|^2 \sin^2 \iota (1 + \cos^2 \iota), \quad (60)$$

$$F_{2\Omega}(\iota) = \frac{4}{15} \frac{\Omega^6}{r^2} |Q_{22}|^2 [(1 + \cos^2 \iota)^2 + 4 \cos^2 \iota]. \quad (61)$$

When integrated over the sphere the corresponding total luminosities are

$$\dot{E}_{\Omega} = \frac{4\pi}{75} \Omega^6 |Q_{21}|^2, \quad (62)$$

$$\dot{E}_{2\Omega} = \frac{256\pi}{75} \Omega^6 |Q_{22}|^2. \quad (63)$$

As noted by Ushomirsky, Cutler & Bildsten (2000), for a given magnitude of the quadrupole moment, a Q_{22} perturbation is 64 times more luminous than a Q_{21} perturbation.

However, in terms of detectability, the relevant quantity is not the energy flux but the signal-to-noise ratio, which is linear in the gravitational wave amplitude (Jaranowski, Królak & Schutz 1998). For a star radiating continuously at gravitational wave frequencies Ω and 2Ω , Jaranowski, Królak & Schutz (1998) showed that the signal-to-noise is

$$d = \sqrt{d_1^2 + d_2^2}, \quad (64)$$

where

$$d_1 = \frac{2}{S_h(\Omega)} \int h_1^2(t) dt, \quad (65)$$

$$d_2 = \frac{2}{S_h(2\Omega)} \int h_2^2(t) dt. \quad (66)$$

In this equation, the time integral is over the duration of the observation, $S_h(f)$ is the detector's noise spectral density, and $h_1(t), h_2(t)$ are defined in terms of the beam functions of equation (46):

$$h_1(t) = F_+(t)h_+^{\Omega}(t) + F_{\times}(t)h_{\times}^{\Omega}(t) \quad (67)$$

$$h_2(t) = F_+(t)h_+^{2\Omega}(t) + F_{\times}(t)h_{\times}^{2\Omega}(t). \quad (68)$$

The wave amplitudes $h_+^{\Omega}(t), h_{\times}^{\Omega}(t), h_+^{2\Omega}(t), h_{\times}^{2\Omega}(t)$ are given in equations (42)–(45). In the case of gravitational wave searches at a single frequency from a known pulsar, it was found that a signal-to-noise threshold of 11.4 was necessary to achieve a false alarm probability of 1% and a false dismissal probability of 10% (Abbott et al. 2004). This signal-to-noise threshold will have to be recalculated for a two-frequency search; we will discuss this further in section 7.

The value of the signal-to-noise for a particular star, and the relative importance of the two harmonics, depends upon all 10 of the parameters given in equation (55). In order to gain a *rough* idea of the relative importance of the two harmonics, we will define an approximate signal-to-noise ratio for each according to

$$\rho = \frac{h\sqrt{T_{\text{obs}}}}{\sqrt{S_h(f_{\text{GW}})}}, \quad (69)$$

where T_{obs} is the duration of the observation (see Jaranowski, Królak & Schutz (1998) for a justification of the scaling with observation time). For the gravitational wave amplitude h we will take the square root of the time-averaged sum of the squares of the plus and cross gravitational wave polarisations, i.e.

$$h = \langle (h_+)^2 + (h_{\times})^2 \rangle^{1/2}, \quad (70)$$

where the angle brackets denote time averaging. Then equation (59) gives

$$h \equiv \langle (h_+)^2 + (h_{\times})^2 \rangle^{1/2} = \frac{4}{\Omega_{\text{GW}}} \sqrt{\pi F}, \quad (71)$$

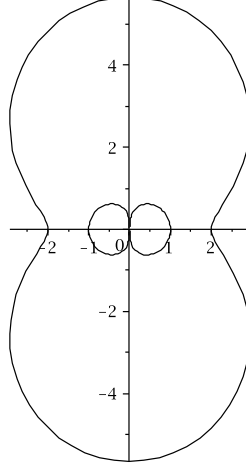


Figure 2. Contour plot showing normalised signal strengths of the Ω (inner contour) and 2Ω (outer contour) harmonics, assuming $|Q_{21}| = |Q_{22}|$. For the Ω radiation we plot $\sin \iota (1 + \cos \iota)^{1/2}$, for the 2Ω radiation $2[(1 + \cos \iota)^2 + 4 \cos^2 \iota]^{1/2}$. The rotation axis ($\iota = 0$) lies along the vertical.

allowing us to write the signal-to-noise ratios for the two harmonics as

$$\rho_{\Omega}(\iota) = \frac{A}{\sqrt{S_h(\Omega)}} |Q_{21}| \sin \iota (1 + \cos \iota)^{1/2}, \quad (72)$$

$$\rho_{2\Omega}(\iota) = \frac{2A}{\sqrt{S_h(2\Omega)}} |Q_{22}| [(1 + \cos \iota)^2 + 4 \cos^2 \iota]^{1/2}, \quad (73)$$

where

$$A = 2 \left(\frac{\pi}{15} \right)^{1/2} T_{\text{obs}}^{1/2} \Omega^2. \quad (74)$$

To compare the relative signal strengths of these harmonics, the inclination angle-dependent coefficients of $A|Q|^2/S_h(f)$ appearing in the above equations are presented in Figure 2. The Q_{21} multipole emits preferentially in the rotational equator ($\iota = \pi/2$), emitting no radiation along the rotation axis ($\iota = 0$), while the Q_{22} emits preferentially along the rotation axis, with a non-zero wave amplitude in all directions. Clearly, for all observer locations and for $|Q_{21}| = |Q_{22}|$, the 2Ω radiation is stronger than the Ω radiation. The ratio of the sky-averaged gravitational waves strengths (as defined in equation (71)) is approximately $3.9 \approx 4$. Of course, the ratio of the possible maximum signal-to-noise ratios would also fold in the frequency dependence of the detector noise between frequencies Ω and 2Ω .

If instead we were to place an upper limit on the wave amplitude of a star known to be losing kinetic energy at a rate \dot{E} , then equations (62) and (63) show that the upper limits on the multipoles stand in the ratio $|Q_{21}^{\text{max}}| = 8|Q_{22}^{\text{max}}|$ (Ushomirsky, Cutler & Bildsten 2000). It then follows that a star losing energy at a known rate is, when sky-averaged, $8/3.9 \approx 2$ times stronger in gravitational wave amplitude if it emitting via a pure Q_{21} multipole than when emitting via a Q_{22} multipole. Such an upper limit is appropriate for known pulsars of measured spin-down rate (if one assumes all of the kinetic energy being lost is converted into gravitational wave emission), or for low-mass X-ray binaries of known X-ray luminosity (if one assumes the spin-up accretion torque, as estimated from the X-ray luminosity, is balanced by a spin-down gravitational torque).

4 EXTENSION TO AN ELASTIC STAR

It is straightforward to allow for the rotationally-induced deformation of the star by adding terms to the moment of inertia tensor. For the crust we amend equation (1) to

$$I_{ab}^C = I_1^C n_a^1 n_b^1 + I_2^C n_a^2 n_b^2 + I_3^C n_a^3 n_b^3 + \Delta I_{\Omega}^C n_a^C n_b^C, \quad (75)$$

where n_a^C is a unit vector pointing along Ω_a^C . Physically, the term $\Delta I_{\Omega}^C n_a^C n_b^C$ represents a deformation biaxial about Ω_a^C , and ΔI_{Ω}^C is numerically equal to the difference in moments of inertia about axes parallel and orthogonal to the Ω_a^C induced by the rotation. The terms in I_1^C , I_2^C and I_3^C give the moment of inertia of the star in the absence of rotation. The differences I_{31}, I_{32}, I_{21} are defined as before (equations (17)–(19)) and can be non-zero only by virtue of non-rotational forces, e.g. elastic or magnetic strains.

A similarly decomposition applies for the superfluid:

$$I_{ab}^{\text{SF}} = I^{\text{SF}} \delta_{ab} + \Delta I_{\Omega}^{\text{SF}} n_a^{\text{SF}} n_b^{\text{SF}}, \quad (76)$$

where n_a^{SF} is a unit vector along Ω_a^{SF} . The star's angular momentum components then become

$$J_1 = (I_1^{\text{C}} + \Delta I_{\Omega}^{\text{C}}) \Omega_1^{\text{C}} + (I^{\text{SF}} + \Delta I_{\Omega}^{\text{SF}}) \Omega_1^{\text{SF}}, \quad (77)$$

$$J_2 = (I_2^{\text{C}} + \Delta I_{\Omega}^{\text{C}}) \Omega_2^{\text{C}} + (I^{\text{SF}} + \Delta I_{\Omega}^{\text{SF}}) \Omega_2^{\text{SF}}, \quad (78)$$

$$J_3 = (I_3^{\text{C}} + \Delta I_{\Omega}^{\text{C}}) \Omega_3^{\text{C}} + (I^{\text{SF}} + \Delta I_{\Omega}^{\text{SF}}) \Omega_3^{\text{SF}}. \quad (79)$$

These are identical in form to the corresponding rigid star equations, (4)–(6), the mapping from the rigid star to elastic star equations being $I_1^{\text{C}} \rightarrow I_1^{\text{C}} + \Delta I_{\Omega}^{\text{C}}$ (and similarly for $I_2^{\text{C}}, I_3^{\text{C}}$) and $I^{\text{SF}} \rightarrow I^{\text{SF}} + \Delta I_{\Omega}^{\text{SF}}$. It follows at once that the solutions, both precessional and non-precessional, are of the same form for this more realistic elastic model as for the rigid star.

There will however be a change in the corresponding gravitational wave emission, as we must now include the contributions from the mass asymmetries associated with the $\Delta I_{\Omega}^{\text{C}}$ and $\Delta I_{\Omega}^{\text{SF}}$ components. For the non-precessional solution it is easy to convince oneself that the impact on the gravitational wave emission is minimal. The Ω_a^{C} vector points along the invariant angular momentum axis, so there is no gravitational wave emission from the $\Delta I_{\Omega}^{\text{C}}$ term. The $\Delta I_{\Omega}^{\text{SF}}$ piece represents a biaxial deformation about Ω_a^{SF} , which is misaligned with the angular momentum axis. This piece therefore does radiate. Rather than calculating this contribution fully, we can make a simple estimate. This deformation is of size $\Delta I_{\Omega}^{\text{SF}}$ and moves at a rate Ω in a cone of half-angle $\cos^{-1}(n_a^J n_a^{\text{SF}})$ about n_a^J , the unit vector in the direction of J_a . Using the results of section 2, a little algebra leads to

$$\cos^{-1}(n_a^J n_a^{\text{SF}}) \approx \frac{\sin \theta^{\text{SF}} [\cos^2 \theta^{\text{SF}} (I_{31} \cos^2 \phi^{\text{SF}} + I_{32} \sin^2 \phi^{\text{SF}})^2 + (I_{21} \sin \theta^{\text{SF}} \sin \phi^{\text{SF}} \cos \phi^{\text{SF}})^2]^{1/2} \Omega_3^{\text{C}}}{I^{\text{SF}} \Omega_3^{\text{SF}}}, \quad (80)$$

where we have worked to leading order in the small quantities of equation (34). We see that Ω_a^{SF} lies very close to J_a ; for $\Omega_3^{\text{C}} \approx \Omega_3^{\text{SF}}$ we obtain

$$\cos^{-1}(n_a^J n_a^{\text{SF}}) \sim \frac{\Delta I}{I^{\text{SF}}}, \quad (81)$$

where we have defined

$$\Delta I = \max(I_{21}, I_{31}, I_{32}). \quad (82)$$

It follows that the $\Delta I_{\Omega}^{\text{SF}}$ term produces a gravitational wave field of a similar form to the I_{31} term in equations (50)–(53), but with the replacements $I_{31} \rightarrow \Delta I_{\Omega}^{\text{SF}}$ and $\theta \rightarrow \Delta I/I^{\text{SF}}$. It follows that the contribution of this component to the gravitational wave emission is weaker than that of the crust as calculated in equations (50)–(53) by a factor $\Delta I_{\Omega}^{\text{SF}}/I^{\text{SF}}$. For all realistic scenarios this ratio will be much less than unity, so we will therefore not consider this component of the wave emission in the remainder of this paper. We therefore see that allowance for rotational deformation of the non-precessing star has minimal impact on the gravitational wave emission.

5 LIMITATIONS AND CAVEATS

What limits the maximum gravitational wave amplitude? In the absence of the pinned superfluid component the answer has been obtained by Ushomirsky, Cutler & Bildsten (2000): the Q_{22} multipole is limited by the breaking strain u_{break} of the crust:

$$Q_{\text{max}} \approx 1.2 \times 10^{39} \text{ g cm}^2 \left(\frac{u_{\text{break}}}{10^{-1}} \right), \quad (83)$$

(see also Haskell et al. (2006)). Also, as discussed in the conclusions section of Ushomirsky, Cutler & Bildsten (2000), an identical limit is placed on Q_{21} . (That these bounds are identical can be understood by noting that the real parts of Y_{22} and Y_{21} density perturbations are identical up to a rotation of axes). So, if the ability of the crustal strain to produce the asymmetries I_{21}, I_{31}, I_{32} were the only factor, the upper bounds on the signal strengths would be given by equation (72) with $|Q_{21}| = Q_{\text{max}}$ for a pure Q_{21} deformation, and by equation (73) with $|Q_{22}| = Q_{\text{max}}$ for a pure Q_{22} deformation. In the general case of a mixed Q_{21}, Q_{22} deformation, both perturbations contribute to the strain field, and the limit on each is reduced (Ushomirsky, Cutler & Bildsten 2000).

However, the presence of the pinned superfluid complicates this picture. In our model, there is an angular velocity misalignment between the superfluid and the rest of the star, as calculated above (equation 81). It follows that over the pinning region the crust exerts a force on the superfluid, supplying the torque required to allow for its time-varying angular velocity. As is demonstrated in appendix A, this torque is supplied by the Magnus force, generated by the flow of superfluid past the pinned vortices. It follows that there are new failure mechanisms as compared to the case studied by Ushomirsky, Cutler & Bildsten (2000). Firstly, the pinning force interaction between the solid crust and the vortices has to be sufficiently strong that the vortices don't unpin. Secondly, the corresponding equal but opposite force on the crust will strain it further.

This additional strain might push the crust closer to, or beyond, its breaking strain. This will also produce some change in the moment of inertia tensor, potentially modifying the gravitational wave emission. Finally, there is also the possibility that relative flow between the superfluid and the vortices may trigger an instability. Let us make some simple estimates of the importance of these effects.

To do so, note that we could set our star up with an arbitrarily large difference between Ω_a^{SF} and Ω_a^{C} . However, in the physically most plausible case, these two vectors will be of equal magnitudes, but misaligned by the angle $\cos^{-1}(n_a^J n_a^{\text{SF}})$, producing a vortex–superfluid relative velocity of order

$$\Delta v \sim \Omega R \cos^{-1}(n_a^J n_a^{\text{SF}}), \quad (84)$$

where R is the stellar radius. Equation (81) then leads to

$$\Delta v \sim \Omega R \frac{\Delta I}{I^{\text{SF}}}. \quad (85)$$

Parameterising:

$$\Delta v \sim 6 \times 10^4 \text{ cm s}^{-1} \left(\frac{f}{\text{kHz}} \right) \left(\frac{\Delta I/I}{10^{-7}} \right) \left(\frac{10^{-2}}{I^{\text{SF}}/I} \right) \left(\frac{R}{10^6 \text{ cm}} \right), \quad (86)$$

where $f = \Omega/(2\pi)$, and I denotes the total stellar moment of inertia. This will be useful in interpreting some of the estimates that follow. This can equivalently be restated in terms of a pinning force per unit length of vortex (Link & Cutler 2002):

$$f_a = \rho^{\text{SF}} \kappa \epsilon_{abc} n_b^{\text{SF}} (v_c^{\text{SF}} - v_c^{\text{C}}) \quad (87)$$

where ρ^{SF} is the superfluid density and κ the quantum of vorticity. Writing the relative velocity using equation (85) gives

$$f \sim 1.3 \times 10^{16} \text{ dyn cm}^{-1} \left(\frac{f}{\text{kHz}} \right) \left(\frac{\Delta I/I}{10^{-7}} \right) \left(\frac{10^{-2}}{I^{\text{SF}}/I} \right) \left(\frac{\rho^{\text{SF}}}{10^{14} \text{ g cm}^{-3}} \right) \left(\frac{R}{10^6 \text{ cm}} \right). \quad (88)$$

These equations give the relative vortex–superfluid velocities, or, equivalently, the pinning forces per unit length of vortex, required to sustain the non-precessional solutions described in this paper.

5.1 Breaking the pinning

First let us ask if the pinning is strong enough to withstand the Magnus force. There exist both observational and theoretical inputs to this issue. On the observational side, glitches and neutron star precession may tell us something about the pinning strength, while, on the theoretical side, there has been some microphysical modelling of how vortices interact with the rest of the star.

Let us start with the observations of glitching pulsars. The smaller glitches, such as those seen in the Crab, may be caused by ‘starquakes’, i.e. changes in the elastic strain of the crust, and so may not carry information about the superfluid pinning. However, the larger so-called ‘giant glitches’, such as those in the Vela pulsar, are believed to represent sudden unpinning events. An estimate of the relative superfluid–vortex velocity at unpinning comes from assuming angular momentum conservation (Link & Cutler 2002; Glampedakis & Andersson 2009). If the glitch represents a sudden angular momentum exchange between the pinned superfluid and the rest of the star (in our language the ‘crust’), then the changes in angular frequency of these two components are related via $I^{\text{SF}} \Delta \Omega^{\text{SF}} + I^{\text{C}} \Delta \Omega^{\text{C}} = 0$. Observations indicate that, when averaged over many glitches, a few percent of the total spin-down is reversed in glitches (Lyne & Graham-Smith 1998), corresponding to $I^{\text{SF}}/I^{\text{C}} \approx 10^{-2}$. It follows we can estimate the pre-glitch velocity lag by

$$\Delta v \approx \Delta \Omega^{\text{SF}} R \approx \frac{I^{\text{C}}}{I^{\text{SF}}} \Delta \Omega^{\text{C}} R, \quad (89)$$

where the quantity $\Delta \Omega^{\text{C}}$ is obtained directly from glitch observations. Parameterising with the Vela in mind:

$$\Delta v \approx 7 \times 10^3 \text{ cm s}^{-1} \left(\frac{10^{-2}}{I^{\text{SF}}/I} \right) \left(\frac{\Delta \Omega^{\text{C}}}{7 \times 10^{-5} \text{ Hz}} \right). \quad (90)$$

Comparing with equation (86), we see that this is smaller than the relative velocity needed to sustain our non-precessing stars, for at least some part of the potential parameter space (viz rapidly spinning stars with large deformations and low pinned superfluid fractions). However, it is likely that (90) is too conservative an estimate on the critical velocity for unpinning. Firstly, the estimate assumes that the velocity difference is reset to zero at the glitch. If only some of the velocity difference is relieved, a larger critical velocity would be obtained. Secondly, glitches presumably involve the most weakly pinned superfluid (in a spinning down star, the weaker pinning sites will break before the stronger ones), whereas it is the strongest pinning locations that matter in building our non-precessional solutions. So, it is not clear if the relative velocity of equation (90) limits the allowed vortex–superfluid velocities in neutron stars.

Turn now to free precession. The free precession period of a neutron star in the absence of superfluid pinning is given approximately by $P_{\text{fp}} \sim PI/\Delta I$ (Landau & Lifshitz 1976), while the precession period with pinning is approximately $P_{\text{fp}} \sim PI/I^{\text{SF}}$ (Shaham 1977). Given that we expect $\Delta I \ll I^{\text{SF}}$, it follows that the precession period is much shorter in the case of superfluid pinning than without pinning. It follows that an observation of free precession would yield an insight into the stellar interior. Unfortunately, free precession does not seem to be a common phenomenon in the pulsar population. The most convincing observation is of approximately 500 day precession in PSR B1828-11 (Stairs et al. 2000), but more recent observations of this and other objects may cast doubt on the precessional interpretation (M. Kramer, personal communication). Nevertheless, if interpreted as precession, the long 500 day period implies that there is no significant pinned superfluid component in the precessing star. As discussed by Link (2003, 2006), this may have significant repercussion for the nature of superconductivity in the stellar core (but see Glampedakis, Andersson & Jones (2008, 2009) for a counterargument). What does seem likely is that, if PSR B1828-11 really is precessing, the precessional motion itself must have set up a velocity field that has caused large scale unpinning (Link & Cutler 2002). It follows that one can estimate the critical velocity to up-pin even the strongest pinned vortices by examining the relative flow in a precessing neutron star with superfluid pinning. The velocity field is of order (Glampedakis, Andersson & Jones 2009)

$$\Delta v \leq \Omega R \theta \frac{I^{\text{SF}}}{I}, \quad (91)$$

where θ , the ‘wobble angle’, can be estimated from observations (Jones & Andersson 2001; Link & Epstein 2001). Parameterising in terms of PSR B1828-11:

$$\Delta v(\text{PSR B1828} - 11, \text{ precession}) \leq 8.1 \times 10^3 \text{ cm s}^{-1} \left(\frac{R}{10^6 \text{ cm}} \right) \left(\frac{\theta}{3^\circ} \right) \left(\frac{I^{\text{SF}}/I}{10^{-2}} \right). \quad (92)$$

Comparing with equation (86) we see that this critical velocity is low enough to be problematic for some portion of the parameter space of interest for our non-precessing solutions, specifically very rapidly rotating stars with small superfluid fractions.

Finally let us turn to theoretical estimates of the strength of pinning. In the case of pinning in the inner crust, Link (2009) recently examined the problem of how a vortex embedded in a nuclear lattice responds to a superfluid flow. Link solved the equation of motion of a single vortex, including tension, Magnus and drag terms. He found that when the relative vortex-superfluid velocity lay below a critical value the vortex essentially remained bound to the nuclei, i.e. the perfect pinning regime applied. Using recent calculations of the vortex-nucleus interaction energy (Donati & Pizzochero 2006) Link estimated

$$\Delta v(\text{crust, theory}) \approx 10^6 - 10^7 \text{ cm s}^{-1}. \quad (93)$$

Comparing (93) and (86) indicates that, by Link’s calculation at least, our non-precessing stars are safely in the regime of perfect pinning in the inner crust. As discussed by Link (2009), this velocity difference is large enough to allow the necessary accumulation of differential rotation to explain giant glitches, but too large to be consistent with an observation of slow free precession. In the case of pinning in the core, Link (2003) estimates a maximum pinning force of $3 \times 10^{15} B_{12}^{1/2} \text{ dyn cm}^{-1}$, or in terms of a relative velocity,

$$\Delta v(\text{core, theory}) \approx 5 \times 10^3 \text{ cm s}^{-1} \left(\frac{B}{10^{12} \text{ G}} \right)^{1/2} \left(\frac{3 \times 10^{14} \text{ g cm}^{-3}}{\rho^{\text{SF}}} \right). \quad (94)$$

Comparing with equation (86) we see that, by this estimate at least, the core vortex-fluxtube interaction may not be strong enough to sustain pinning for non-precessing stars with high spin frequencies and small superfluid fractions, and the problem is more severe for weakly magnetised stars.

To sum up, the critical unpinning velocities implied by observations suggest that unpinning may be a problem for our non-precessional solutions, but only for very rapidly spinning stars with relatively small pinned superfluid fractions. Slower spinning stars, or stars with larger pinned superfluid fractions, should be immune from Magnus-force generated unpinning. Theoretical estimates, on the other hand, suggest that all non-precessional solutions should be safe from unpinning in the inner crust. Alternatively, one can note that an observation of a non-precessing star radiating gravitationally at Ω and 2Ω would imply that the bounds on the critical unpinning velocity from glitches and precession (equations 90 and 92) are not reliable.

5.2 Changes in shape

Now let us examine the change in shape of the star in response to the pinning forces. We will consider the cases of elastic and magnetic deformation separately.

Let us begin with a star deformed by a magnetic field of strength $\sim B$. The deformation ΔI will be sourced by a magnetic stress of order B^2 , and, to a rough approximation, the fractional deformation $\Delta I/I$ will be of order of the ratio of magnetostatic and gravitational binding energies (Jones 2002):

$$\frac{\Delta I}{I} \sim \frac{B^2 R^3}{GM^2/R}. \quad (95)$$

The Magnus force will perturb the star, resulting in a magnetic stress perturbation of order $B\delta B$, and so a magnetic force per unit volume $\sim B\delta B/R$. This balances the Magnus force per unit volume of $\rho^{\text{SF}} R\Omega^2 \Delta I/I^{\text{SF}}$. Combining these results, and simplifying using $I^{\text{SF}} \sim \rho^{\text{SF}} R^5$ leads to

$$\frac{\delta B}{B} \sim \frac{I\Omega^2}{GM^2/R}. \quad (96)$$

This is the ratio of the rotational kinetic energy to the gravitational binding energy, and will be much less than unity for all but the most rapidly rotating stars. We can therefore conclude that, in the case of a magnetically deformed star, the change in magnetic field, and therefore shape, caused by the pinning forces is small.

A very similar calculation applies if we assume the pinning occurs in a crustal shell of thickness ΔR , shear modulus μ , subject to a strain u . The deformation $\Delta I/I$ will be sourced by an elastic stress of order μu , and, to a rough approximation, $\Delta I/I$ will be of order of the ratio of Coulomb binding energy to gravitational binding energy, multiplied by the strain (Jones 2002):

$$\frac{\Delta I}{I} \sim \frac{\mu R^2 \Delta R}{GM^2/R} u. \quad (97)$$

The Magnus force will perturb the crust, resulting in an elastic stress of order $\mu\delta u$, and so an elastic force per unit volume of $\mu\delta u/\Delta R$. This balances the Magnus force per unit volume $\rho^{\text{SF}} R\Omega^2 \Delta I/I^{\text{SF}}$. Combining these results, and simplifying using $I^{\text{SF}} \sim \rho^{\text{SF}} R^4 \Delta R$ leads to

$$\frac{\delta u}{u} \sim \frac{\Delta R}{R} \frac{I\Omega^2}{GM^2/R}. \quad (98)$$

This is a factor $\Delta R/R$ smaller than the corresponding magnetic result, showing that, in the elastic case, the pinning forces have minimal impact on the strain distribution.

We can therefore conclude that pinning forces do not significantly alter the shape of our star. This means there is no danger of the pinning inducing fracture, and also that the gravitational wave field calculated previously is not significantly modified by Magnus force-induced shape changes.

5.3 Superfluid instabilities

We can also ask whether or not a superfluid vortex instability might be induced, of the form investigated recently by several authors (Peralta et al. 2006; Sidery, Andersson & Comer 2008). The instability occurs in stars consisting of two fluid components: a superfluid neutron component, and a charged component, coupled via the mutual friction force. When the coupling between superfluid vortices and the star's charged components is sufficiently strong, a relative flow of superfluid along the vortex array induces an inertial plane wave instability. In particular, Glampedakis, Andersson & Jones (2008, 2009) showed that such an instability would be triggered in a precessing star, if the wobble angle were sufficiently large. Could such an instability be triggered by the angular velocity mismatch in our non-precessing star?

Taking the strong pinning limit of Glampedakis, Andersson & Jones (2009) (their equations (46) and (47)) and writing the relative flow of superfluid along vortices, w , as $w \approx \Omega R \Delta I/I_{\text{SF}}$ as given in equation (85), we find that there do indeed exist unstable plane wave solutions; see appendix B for details. These occur for wavelengths smaller than a critical value: $\lambda_{\text{crit}} \approx \pi R \Delta I/I_{\text{SF}}$:

$$\lambda^{\text{critical}} \approx 30 \text{ cm} \left(\frac{R}{10^6 \text{ cm}} \right) \left(\frac{\Delta I/I}{10^{-7}} \right) \left(\frac{10^{-2}}{I^{\text{SF}}/I} \right). \quad (99)$$

This wavelength is longer than the inter-vortex separation in all stars of interest (Sauls 1989):

$$\Delta x^{\text{vortex}} \approx 10^{-2} \text{ cm} \left(\frac{\text{Hz}}{f} \right)^{1/2}, \quad (100)$$

leaving a range of wavelengths where the instability could be operative. As shown in appendix B, the fastest growing perturbation has a wavelength of approximately $\lambda^{\text{critical}}/2$, and a corresponding growth time of

$$\tau \approx 0.1 \text{ s} \left(\frac{100 \text{ Hz}}{f} \right)^2 \left(\frac{10^8 \text{ K}}{T} \right)^2 \left(\frac{x_p}{0.1} \right) \left(\frac{10^6 \text{ cm}}{R} \right)^2 \left(\frac{I^{\text{SF}}/I}{10^{-2}} \right)^2 \left(\frac{10^{-7}}{\Delta I/I} \right)^2. \quad (101)$$

In this equation x_p denote the ratio of the proton to neutron densities, and the temperature T enters as the instability is sensitive to the temperature dependent electron-electron shear viscosity. These results indicate that the superfluid instability may be operative in stars of gravitational wave interest. If so, the instability could potentially unpin the vortices and,

presumably, eliminate the misalignment between superfluid and crustal principal axis necessary for our wave generation mechanism, eliminating the multiple harmonic gravitational wave emission.

However, van Hoven & Levin (2008) have recently argued that the inclusion of hydromagnetic forces acts to stabilise the instability. They found that, when such forces were included, the relative velocity needed for instability was $(BB_{\text{cr}}/\pi\rho^{\text{SF}})^{1/2}$, where $B_{\text{cr}} \approx 10^{15}$ G is the critical magnetic field confined to the flux tubes. Combining with our relative velocity $w \approx \Omega R \Delta I / I^{\text{SF}}$ allows us to estimate the spin frequency *above* which this inertial wave instability would operate:

$$f \approx 3 \times 10^4 \text{ Hz} \left(\frac{10^6 \text{ cm}}{R} \right) \left(\frac{10^{-7}}{\Delta I / I} \right) \left(\frac{I^{\text{SF}} / I}{10^{-2}} \right) \left(\frac{10^{14} \text{ g cm}^{-3}}{\rho^{\text{SF}}} \right)^{1/2} \left(\frac{B}{10^{12} \text{ G}} \right)^{1/2}. \quad (102)$$

This is very high, indicating that the magnetohydrodynamic forces might indeed be effective in suppressing the instability in all but the most weakly magnetised stars.

To sum up, the multipole moments Q_{21} and Q_{22} that generate our gravitational wave field will be bounded by the crust's finite shear modulus and breaking strain, as described by Ushomirsky, Cutler & Bildsten (2000). There are other possible failure mechanisms connected with the finite strength of the pinning and a possible vortex instability. Depending upon the detailed (and poorly understood) physics of the amount and location of the pinned superfluid and the pinning strength, these failure mechanism could potentially prevent the creation of a steadily rotating Q_{21} mass quadrupole. Conversely, observation of gravitational radiation at the two frequencies $(\Omega, 2\Omega)$ would imply that these failure mechanism are not operative.

6 OTHER FREQUENCY SPLITTING MECHANISMS

There exists (at least) two other ways in which an apparently steadily spinning star might emit at both Ω and 2Ω , even without a pinned superfluid component. We will comment on these mechanisms briefly, and argue that they are much less efficient than superfluid pinning in producing the double frequency emission.

6.1 Free precession of a biaxial star

Consider a perfectly biaxial star, i.e. one with moment of inertia tensor of the form

$$I_{ab} = I_0 \delta_{ab} + \Delta I n_a n_b. \quad (103)$$

As is well known the free precession of such an object is very simple, consisting of the superposition of two steady rotations: the symmetry axis n_a rotates about the fixed angular momentum vector with period $\sim P$, with a superposed slow ($P_{\text{fp}} \sim P I_0 / \Delta I$) rotation about the symmetry axis (Landau & Lifshitz 1976). If the pulsar beam lies exactly along n_a , and if the beam is exactly axisymmetric about n_a , then the radio pulsations will be steady at period P , with no precessional modulation (Jones & Andersson 2001). The gravitational wave emission is insensitive to the superimposed slow rotation, and has the form given by equations (50)–(53), with $I_{31} = \Delta I$ (Zimmermann & Szedenits, Jr. 1979; Jones & Andersson 2002). This is the sort of motion modelled in Gal'tsov, Tsvetkov & Tsirulev (1984), Bonazzola & Gourgoulhon (1996), Melatos & Payne (2005), and Vigelius & Melatos (2009), where a magnetic field sources the deformation ΔI ; see section 7 for discussion.

However, this is clearly a very special case. Firstly, it is unlikely that the moment of inertia tensor is biaxial around the magnetic axis. Crustal contributions are likely to be misaligned from the magnetic ones, particularly if the crust retains any memory of a relaxed shape from a previous higher rotation rate (Culter, Ushomirsky & Link 2003), and any significant contribution to I_{ab} not of the form $\Delta I n_a n_b$ would make the inertia tensor triaxial, breaking the symmetry and introducing detectable periodicities into the observed rotation (Zimmermann & Szedenits, Jr. 1979; Zimmermann 1980; Van Den Broeck 2005). Secondly, pulsation profiles are known to be non-axisymmetric, as evidenced by the complexity of pulse profiles (Lyne & Graham-Smith 1998). Finally, the precession motion would damp on some dissipative timescale, so would not be long-lived (Sedrakian, Wasserman & Cordes 1999; Cutler 2002). We therefore feel that such a motion is unlikely to be common in the pulsar population.

6.2 Electromagnetic torques

Magnetised neutron stars are acted upon by an electromagnetic torque. The torque consists of the familiar spin-down torque, scaling as Ω^3 , and also a so-called anomalous torque, a factor $c/(\Omega R)$ larger than the spin-down torque, scaling as Ω^2 (Goldreich 1970):

$$T_a = \frac{\alpha}{R c^2} (\Omega_d^C m_d) \epsilon_{abc} \Omega_b^C m_c, \quad (104)$$

where m_a is the star's dipole moment and α a factor of order unity, which Goldreich (1970) sets to unity, but Good & Ng (1985) correct to $-1/5$. This torque is orthogonal to Ω_a^C and so does no work on the star. However, it can have an affect upon

the rotation (Goldreich 1970; Melatos 2000). To see this, look at the special case of a star with a biaxial deformation ΔI^C caused by crustal strain and a biaxial deformation ΔI^B caused by magnetic fields:

$$I_{ab} = I_0 \delta_{ab} + \Delta I^C n_a^C n_b^C + \Delta I^B n_a^B n_b^B, \quad (105)$$

where the unit vectors n_a^C and n_a^B define the symmetry axes of the crustal and magnetic deformations, respectively. The Euler equation of motion in the presence of a torque T_a is

$$\frac{dJ_a}{dt} + \epsilon_{abc} \Omega_b^C J_c = T_a. \quad (106)$$

Combining the above equations and selecting the non-precessional solution by setting $dJ_a/dt = 0$ we obtain

$$\Delta I^C (n_d^C \Omega_d^C) \epsilon_{abc} \Omega_b^C n_c^C + \Delta I^B (n_d^B \Omega_d^B) \epsilon_{abc} \Omega_b^B n_c^B = A (\Omega_d^C n_d^B) \epsilon_{abc} \Omega_b^C n_c^B, \quad (107)$$

where $m_a = m n_a^B$ and

$$A = \frac{\alpha m^2}{R c^2}. \quad (108)$$

As noted by Goldreich (1970), this torque can be absorbed into the moment of inertia tensor:

$$\epsilon_{abc} \Omega_b^C [\Delta I^C (n_d^C \Omega_d^C) n_c^C + (\Delta I^B - A) (n_d^B \Omega_d^B) n_c^B] = 0. \quad (109)$$

It follows that the non-precessional solution is misaligned with the principal axes of I_{ab} by an angle of order

$$\delta\theta \sim \frac{A}{\Delta I}. \quad (110)$$

This misalignment will create a non-axisymmetric mass distribution and lead to gravitational wave emission. That electromagnetic torques have this effect was noted by Sedrakian, Wasserman & Cordes (1999), who considered the effect of the non-anomalous spin-down torque; the principle is exactly the same.

To gauge the significance of this, note that the magnetic moment m is related to the (surface) magnetic field strength via $m \sim BR^3$, and, the magnetic deformation scales as $\Delta I^B \sim B^2 R^6 / (GM)$, so that

$$A \sim \frac{R_{\text{Sch}}}{R} \Delta I^B, \quad (111)$$

where $R_{\text{Sch}} \sim GM/(Rc^2)$ is of order the star's Schwarzschild radius. It follows that the misalignment angle is of order

$$\theta \sim \frac{\Delta I^B}{\Delta I} \frac{R_{\text{Sch}}}{R}. \quad (112)$$

It follows that this misalignment is very small unless the magnetic field makes a significant contribution to the moment of inertia tensor, and even in the case $\Delta I^B \sim \Delta I^C \sim \Delta I$ the angle is suppressed by the factor $R_{\text{Sch}}/R \approx 0.2$. We can therefore conclude that the anomalous torque is not as effective as pinned superfluidity in modifying the gravitational wave spectrum.

In fact, there is a further caveat to be attached to this. The above argument shows that there is a misalignment between the spin and principal axes in a steadily spinning star. If the gravitational wave emission is then calculated by integration over the mass distribution, emission at frequencies Ω and 2Ω would be found in the standard way. However, one should presumably include the contributions to the stress-energy tensor from the magnetic field itself in this calculation. One might worry that inclusion of this additional component might eliminate the Ω harmonic. This is clearly an interesting issue, which we will address in a future study.

7 DISCUSSION

Most targeted gravitational wave searches to date have been motivated by the possibility of the stars having ‘mountains’, i.e. non-zero values of the Q_{22} mass multipole moment. Such a deformed star, rotating rigidly about a principal axis, would emit at exactly twice the spin frequency. Radiation at frequency Ω has received relatively little attention. In large part, this is because, in a single component rigid star, the necessary Q_{21} mass multipole moment would require the star to precess, modulating the observed timing of the radio pulses, and there has been little clear sign of such modulation in the radio pulsations of gravitational wave candidates.

In this paper we have argued that a neutron star containing a pinned superfluid component can rotate in a steady non-precessional way, radiating gravitationally at both Ω and 2Ω , without there being any modulation in the observed radio pulsations. Fundamentally, this is because the pinned superfluid effectively acts as a gyroscope, ‘sewn’ into the crust of the star. This adds an extra piece to the angular momentum, allowing the system’s total angular momentum vector and rotation axis to coincide, even though no one of the crustal principal axes lies along the rotation axis. The superfluid pinning is crucial, and the axis of pinning must not be aligned with a principal axis of the moment of inertia tensor; if it is, the non-precessional

motion is about this axis, and only 2Ω radiation is produced. As we have noted, there exist a number of mechanisms which could break the pinning, depending upon the exact nature of how the superfluid vortices interact with the rest of the star.

What does this mean for gravitational wave search strategies? Clearly, this motivates carrying out gravitational wave searches where data from two harmonics are combined to give a single detection statistic, as described for biaxial precessing stars by Jaranowski, Królak & Schutz (1998). The advantage of such a search over a single frequency search is that it would capture the full radiated signal. However, there is also a disadvantage: the two-harmonic signal is specified by 10 parameters, whereas the conventional single frequency search has only 7 parameters. It is therefore likely that the signal-to-noise threshold necessary to claim a detection would be larger in the two-harmonic search, as the larger parameter space increases the chance of a false detection. Ultimately, just how useful the two-frequency search is compared to the single frequency one will depend upon what sources nature chooses to provide. For a star that radiates only at twice the rotation rate, the two frequency search simply degrades our sensitivity to detection, without adding anything to the signal-to-noise. On the other hand, for a star that radiates appreciably at both harmonics, the two frequency search would surely be an advantage. According to the analysis of section 3.3, the two multipole moments contribute equally to the signal-to-noise ratio when $|Q_{21}| \approx 4|Q_{22}|$ (neglecting the variation in the detector noise with frequency). In the extreme case of a targeted search, if the star radiates only via the Q_{21} multipole, the two frequency search would be essential. Clearly, some numerical experimentation to quantify when you gain and when you lose would be useful. One simple possibility, motivated by the less efficient nature of gravitational wave emission from the Q_{21} moment, would be to search at a single frequency, and only in the event of a detection look for harmonic structure.

However, all of this begs the question: Why should the Q_{21} mass distribution be non-zero? What astrophysical scenario might produce such a state? Unfortunately, this is a far more difficult problem to address. For stars spinning rapidly enough to be of gravitational wave interest, the dominant force deforming neutron stars away from spherical symmetry is rotation, which is necessarily axisymmetric and can only contribute to the (non-radiative) Q_{20} mass multipole. It is therefore not obvious what might lead to a significant non-zero value of Q_{21} . However, exactly the same problem applies in arguing for the existence of a Q_{22} asymmetry. So, by this measure at least, there is no good argument to strongly favour either one of the two sorts of gravitational wave producing asymmetries over and above the other.

One possibility for producing asymmetry is a strong internal magnetic field (Gal'tsov, Tsvetkov & Tsirulev 1984; Bonazzola & Gourgoulhon 1996; Haskell et al. 2008; Cioffi et al. 2009; Lander & Jones 2009). For instance, a magnetic field, symmetric about an axis along n_a^B inclined at an angle χ to the rotation axis, would produce a \hat{Q}_{20} mass multipole when referred to a coordinate system with \hat{z} -axis along direction n_a^B , which, for $0 < \chi < \pi/2$, translates into an χ -dependent linear combination of Q_{20} , Q_{21} , Q_{22} multipole moments, as given by the transformation properties of spherical harmonics under rotation:

$$\hat{Y}_{20} = -\frac{3}{4\sqrt{6}}\sin^2\chi(Y_{22} + Y_{2-2}) - \frac{3}{\sqrt{6}}i\sin\chi\cos\chi(Y_{21} + Y_{2-1}) + \frac{1}{2}(2\cos^2\chi - \sin^2\chi)Y_{20}. \quad (113)$$

However, as is well known, the strong field neutron stars (the magnetars) all rotate too slowly to be of gravitational wave interest, while the more rapidly spinning stars (the young pulsars, the low-mass X-ray binaries (LMXBs), and the millisecond pulsars) have relatively weak external magnetic fields. Clearly, only if the internal magnetic field far exceeds the external one would magnetic deformations be of interest.

Most of the known pulsars do indeed seem to be ‘inclined rotators’, i.e. have magnetic fields that are neither aligned with ($\chi = 0$) nor orthogonal to ($\chi = \pi/2$) the rotation axis. What does this mean for their gravitational wave emission? The answer to this depends upon whether or not there is a pinned superfluid component. In the absence of such a component, there are two possibilities. Firstly, if the magnetic deformation were the only deformation, the star would precess, and either align or go orthogonal on some short timescale, leading to no gravitational wave emission or emission at only 2Ω , respectively (Cutler 2002). Secondly, and more plausibly, there would be a corresponding crustal contribution to the inertia tensor, such that the inclined rotator simply rotates about a principal axis of the total inertia tensor, radiating at 2Ω only. (As discussed in detail by Wasserman (2003), for a given inclination angle χ and a given magnetic deformation, this would require a sufficiently large crustal deformation). However, if there is a pinned superfluid component, then the analysis of this paper applies, the motion is non-precessional, and emission at both Ω and 2Ω is possible, depending upon the orientation of the pinned superfluid with respect to the principal axes of the total inertia tensor.

One particular scenario where magnetic fields might prove to be important is in accreting systems, if magnetic burial of the field takes place, resulting in stars with fast spins, strong internal fields and weak external ones. Such a scenario has been modelled in detail by Melatos & Payne (2005) and Vigeliu & Melatos (2009), who showed that accretion of $\Delta M \sim 2 \times 10^{-3} M_\odot$ was sufficient to generate a mass quadrupole of size $\Delta I/I \approx 2 \times 10^{-5}$, biaxial about the magnetic axis. As noted by the above authors, this would generate a precessing star, radiating gravitational waves at the Ω , 2Ω harmonics.

However, in the absence of superfluid pinning, there is an objection to this scenario. The precessional motion would damp on a timescale much shorter than the timescale on which the magnetic mountain is built: the quadrupole is generated on a timescale related to the accretion rate \dot{M} , roughly $\Delta M/\dot{M} \sim 10^6$ years for a typical LMXB, while the precession period, in the absence of pinned superfluidity, is of order $P/\epsilon \sim 10^2$ seconds. It follows that the quality factor of the precession would have

to be unrealistically large to allow the precession, and therefore the radiation at frequency Ω , to survive (Jones & Andersson 2001; Cutler 2002). This changes completely if a pinned superfluid is added to the model. In this case, the rotation remains close to the superfluid pinning axis, and there is no precession, allowing the inclined biaxial magnetic mountain to radiate continuously at the two frequencies. So, unless there exists some mechanism to maintain the precession, the superfluid pinning model of this paper is essential to realise the long-lived multiple frequency gravitational wave generation described by Melatos & Payne (2005) and Vigeliu & Melatos (2009).

The solid crust is the other possible source of the deformation. As was computed in detail by Culter, Ushomirsky & Link (2003), the crust in a pulsar is likely to have a Q_{20} density perturbation sourced by strains generated by the crust retaining a memory of a relaxed state at a higher rotation rate. If such a star is kicked, precession occurs, generating the familiar gravitational wave field. However, what would generate non-zero Q_{21} (or, for that matter, Q_{22}) for our non-precessing stars? One possibility is that some of the glitches in young stars correspond to starquakes, i.e. sudden cracking events, and that these don't occur in completely axisymmetric way.

In fact, a model of symmetry breaking in starquakes has been developed by Franco, Link & Epstein (2000), who were attempting to explain the permanent increases in spin down rate seen after glitches in the Crab pulsar. Their suggestion was that the crust cracks in a non-axisymmetric way, so that, immediately after the glitch, the spin and principal axes are no longer coincident. They argue that a brief period of precession would follow, which, when damped, would leave the star with a permanently increased angle between the magnetic and spin axes. Crucially, to account for the systematic increase of this angle, Franco et al. argued that the magnetic field itself breaks the axisymmetry in the strain build up, and favours quakes along fault lines which tend to increase the spin axis–magnetic dipole axis angle. Clearly, such non-axisymmetric faulting could, in our pinned superfluid scenario, contribute to building non-zero values of the Q_{21} and Q_{22} multipoles. However, for this to work, the starquake would have to occur without significantly unpinning the superfluid, or at least the pinning would have to reform on a timescale short compared to the timescale on which the precession of the star is damped, or else the system would relax to rotation about a principal axis.

The neutron star crust tectonics model of Ruderman and collaborators provides another possible mechanism of symmetry breaking (Ruderman 1976, 1991a,b). This mechanism makes use of both the magnetic field and the core superfluid. The idea is that as a star spins down and its core superfluid vortices migrate outwards, they interact strongly with the magnetic flux tubes which would thread a type II superconducting core. This places a large strain on the crust. The exact deformation produced (i.e. the sizes of Q_{21} and Q_{22}) would require a detailed calculation, and would depend upon the poorly understood interaction between the vortices and flux tubes (Sidery & Alpar 2009), but Ruderman estimates that the corresponding stresses are large—large enough to shear the crust, and so could be a source of non-axisymmetry.

To sum up, we have argued that pinned superfluidity allows a neutron star of spin frequency Ω to emit steady gravitational wave signals at both Ω and 2Ω , without there being any stellar precession. This motivates gravitational wave searches at both harmonics, even when targeting known pulsars with very smooth timing profiles. The non-detection of such radiation would imply that the necessary gravitational wave generating quadrupole moments aren't created in real stars, and/or the pinning isn't strong enough to support them. More interestingly, the observation of radiation at both harmonics from a non-precessing star would provide evidence in favour of pinned superfluidity within the star.

ACKNOWLEDGEMENTS

The author would like to thank Kostas Glampedakis for stimulating discussions on several of the issues discussed in this paper, and also members of the LSC/Virgo continuous wave group. This work was supported by PPARC/STFC via grant number PP/E001025/1. The author also acknowledges support from COMPSTAR, an ESF Research Networking Programme.

APPENDIX A: THE COUPLING TORQUE

In our model, the superfluid component does not rotate steadily—its angular velocity vector Ω_a^{SF} rotates about the fixed crustal angular velocity vector Ω_a^{C} . In this appendix we will show that the torque required to support this motion is supplied by the Magnus force which couples the superfluid and crustal components via the superfluid vortices.

The superfluid is acted on by a Magnus force (Shaham 1977)

$$f_a = \rho^{\text{SF}} \epsilon_{abc} \omega_b (v_c^{\text{SF}} - v_c^{\text{C}}), \quad (\text{A1})$$

where $v_a^{\text{SF}} = \epsilon_{abc} \Omega_b^{\text{SF}} x_c$ is the superfluid velocity, $v_a^{\text{C}} = \epsilon_{abc} \Omega_b^{\text{C}} x_c$ the crust velocity, and $\omega_a = 2\Omega_a^{\text{SF}}$ the superfluid vorticity. We want to see what sort of torque this produces on the crust:

$$T_a = \int_V \epsilon_{abc} x_b f_c dV. \quad (\text{A2})$$

Combining the above equations and simplifying we find

$$T_a = 2\epsilon_{abc} \int_V \rho^{\text{SF}} x_b x_d dV \Omega_d^{\text{SF}} (\Omega_c^{\text{SF}} - \Omega_c^{\text{C}}). \quad (\text{A3})$$

In spherical symmetry (which we assume for the superfluid) the integral simplifies:

$$\int_V \rho^{\text{SF}} x_b x_d dV = \delta_{bd} \int_V \rho^{\text{SF}} x^2 dV, \quad (\text{A4})$$

while the moment of inertia tensor is, by definition,

$$I_{ab}^{\text{SF}} = \int_V \rho^{\text{SF}} (r^2 \delta_{ab} - x_a x_b) dV, \quad (\text{A5})$$

where $r^2 = x^2 + y^2 + z^2$. Picking out a single component:

$$I_{xx}^{\text{SF}} = \int_V \rho^{\text{SF}} (y^2 + z^2) dV = 2 \int_V \rho^{\text{SF}} x^2 dV, \quad (\text{A6})$$

and so

$$\int_V \rho^{\text{SF}} x_b x_d dV = \delta_{bd} I^{\text{SF}} / 2, \quad (\text{A7})$$

where $I^{\text{SF}} \equiv I_{xx}^{\text{SF}} = I_{yy}^{\text{SF}} = I_{zz}^{\text{SF}}$ is the moment of inertia of the spherical superfluid. Inserting this into (A3) and writing in terms of the superfluid angular momentum $J_a^{\text{SF}} = I^{\text{SF}} \Omega_a$ gives

$$T_a = \epsilon_{abc} \Omega_b^{\text{C}} J_c^{\text{SF}}. \quad (\text{A8})$$

This is exactly the torque required to spin a superfluid of angular momentum J_a^{SF} at a rate Ω_a^{C} , confirming that the Magnus force does indeed supply the necessary torque to provide a self-consistent solution.

APPENDIX B: THE SUPERFLUID INSTABILITY

The short wavelength superfluid instability is described in detail in Glampedakis, Andersson & Jones (2009). The complex plane wave frequencies that apply in the limit of strong vortex drag are given by equations (46) and (47) of their paper. The unstable mode has frequency

$$\sigma \approx \Omega^{\text{SF}} \left(1 - \frac{1}{x_p} \right) + kw + \frac{i}{2} \nu k^2 + \frac{1}{x_p} \left[-\frac{1}{4} (\nu k^2 x_p)^2 + ix_p (x_p - 1) \Omega^{\text{SF}} \nu k^2 + \Omega_{\text{SF}}^2 (1 + x_p)^2 - 2\Omega^{\text{SF}} kw x_p \right]^{1/2}, \quad (\text{B1})$$

where x_p is the ratio of proton to neutron densities, k the wave number, and ν the electron-electron shear viscosity. Taking the limit of small wavelength and retaining the dominant terms in the imaginary part of the mode frequency we find:

$$\Im(\sigma) \approx \frac{2\Omega^{\text{SF}}}{x_p \nu} \left[\frac{2\Omega^{\text{SF}}}{k^2} - \frac{w}{k} \right]. \quad (\text{B2})$$

Inserting the relation $w \approx R\Omega^{\text{SF}} \Delta I / I^{\text{SF}}$ gives

$$\Im(\sigma) \approx \frac{2\Omega^2}{\nu x_p} \left[\frac{2}{k^2} - \frac{R}{k} \frac{\Delta I}{I^{\text{SF}}} \right]. \quad (\text{B3})$$

The mode is unstable for $\Im(\sigma) < 0$, so the plane waves are unstable for wavelength less than a critical value at which $\Im(\sigma) = 0$:

$$\lambda^{\text{critical}} = \pi R \frac{\Delta I}{I^{\text{SF}}}. \quad (\text{B4})$$

Further analysis of (B3) shows that the fastest growing mode has a wavelength $\lambda^{\text{critical}}/2$. Substituting this wavelength into (B3) and inverting gives the mode growth timescale:

$$\tau = \frac{4\nu x_p}{\Omega^2 R^2} \left(\frac{I^{\text{SF}}}{\Delta I} \right)^2. \quad (\text{B5})$$

This gives a good estimate of the growth time of the most unstable mode.

REFERENCES

Abbott B. et al., 2004, Phys. Rev. D, 69, 082004

- Abbott B. et al., 2005a, *Phys. Rev. Lett.*, 94, 181103
- Abbott B. et al., 2005b, *Phys. Rev. D*, 72, 102004
- Abbott B. et al., 2007a, *Phys. Rev. D*, 76, 042001
- Abbott B. et al., 2007b, *Phys. Rev. D*, 76, 082001
- Abbott B. et al., 2008a, *Phys. Rev. D*, 77, 022001
- Abbott B. et al., 2008b, *ApJ*, 683, L45
- Abbott B. et al., 2009a, *Rep. Prog. Phys.*, 72, 076901
- Abbott B. et al., 2009b, *Phys. Rev. D*, 79, 022001
- Abbott B. et al., 2009c, *Phys. Rev. Lett.*, 102, 111102
- Acernese F. et al., 2008, *Class. Quantum Grav.* 25 184001
- Anderson P. W., Itoh N., 1975, *Nature*, 256, 24
- Bonazzola S., Gourgoulhon E., 1996, *Astron. Astrophys.* 312, 675
- Cioffi R., Ferrari V., Gualtieri L., Pons J. A., 2009, *MNRAS*, 397, 913
- Cutler C., 2002, *Phys. Rev. D*, 66, 084025
- Cutler C., Ushomirsky G., Link B., 2003, *ApJ*, 588, 975
- Donati P., Pizzochero P. M., 2006, *Phys. Lett. B*, 640, 74
- Franco L. M., Link B., Epstein R. I., *ApJ*, 2000, 543, 987
- Gal'tsov D. V., Tsvetkov V. P., Tsirulev A. N., 1984, *Sov. Phys. JETP*, 59, 472
- Glampedakis, K., Andersson, N., 2009, *Phys. Rev. Lett.*, 102, 141101
- Glampedakis, K., Andersson, N., Jones, D.I., 2009, *MNRAS*, 394, 1908
- Glampedakis, K., Andersson, N., Jones, D.I., 2008, *Phys. Rev. Lett.*, 100, 081101
- Goldreich P., 1970, *ApJ*, 160, L11
- Good M. L., Hg K. K., 1985, *ApJ*, 299, 706
- Grote H., 2008, *Class. Quantum Grav.*, 25, 114043
- Haskell B., Jones D. I., Andersson N., 2006, *MNRAS*, 373, 1423
- Haskell, B., Samuelsson L., Glampedakis K., Andersson, N., 2008, *MNRAS*, 385, 531
- Horowitz, C. J., Kadau K., 2009, *Phys. Rev. Lett.* 102, 191102
- Jaranowski P., Królak, A., Schutz B. F., *Phys. Rev. D*, 58, 063001
- Jones D. I., 2002, *Class. Quant. Grav.*, 19, 1255
- Jones, D.I., Andersson, N., 2001, *MNRAS*, 324, 811
- Jones, D.I., Andersson, N., 2002, *MNRAS*, 331, 203
- Landau L. D., Lifshitz E. M., 1976, *Mechanics*, 3rd Edition. Butterworth-Heinemann Ltd.
- Lander S. K., Jones D. I., *MNRAS*, 395, 2162
- Link B., 2003, *Phys. Rev. Lett.*, 91, 101101
- Link B., 2006, *Astron. Astrophys.*, 458, 881
- Link B., 2009, *Phys. Rev. Lett.*, 102, 131101
- Link B., Cutler C., 2002, *MNRAS*, 336, 211
- Link B., Epstein R. I., 2001, *ApJ*, 556, 392
- Lyne A. G., Graham-Smith F., 1998, *Pulsar Astronomy*. Cambridge University Press
- Melatos A., 2000, *MNRAS*, 313, 217
- Melatos A., Payne D. J. B., 2005, *ApJ*, 623, 1044
- Peralta C., Melatos A., Giacobello M., Oot A., 2006, *ApJ*, 651, 1079
- Ruderman M., 1976, *ApJ*, 203, 213
- Ruderman M., 1991a, *ApJ*, 366, 261
- Ruderman M., 1991b, *ApJ*, 382, 576
- Sauls, J.A., 1989, in *Timing Neutron stars*, ed. Ogelman H. and van de Heuvel E.P.J. (Kluwer Academic Publishers)
- Sedrakian, A., Wasserman, I., Cordes, J.M., 1999, *Ap. J.* 524, 341
- Shaham J., 1977, *ApJ*, 214, 251
- Shapiro S. L., Teukolsky S. A., 1983, *Black Holes, White Dwarfs, and Neutron Stars*, Wiley-Interscience
- Sidery T., Alpar M. A., 2009, arXiv:0905.3097
- Sidery T., Andersson N., Comer G. L., 2008, *MNRAS*, 385, 335
- Stairs I. H., Lyne A. G., Shemar S. L., 2000, *Nature*, 406, 484
- Thorne K. S., 1980, *Rev. Modern Physics*, 52, 299
- Ushomirsky G., Cutler C., Bildsten L., 2000, *MNRAS*, 319, 902
- Van Den Broeck C., 2005, *Class. Quant. Grav.*, 22, 1825
- van Hoven M., Levin Y., 2008, *MNRAS*, 391, 283
- Vigeliu M., Melatos A., 2009, *MNRAS*, 395, 1972

Wasserman, I., 2003, MNRAS, 341, 1020

Zimmermann M., Szedenits Jr. E., 1979, Phys. Rev. D, 20, 351

Zimmermann M., 1978, Phys. Rev. D, 21, 891